




ORIGINAL RESEARCH



## Reciprocal influence of B cells and tumor macro and microenvironments in the *Apc<sup>Min/+</sup>* model of colorectal cancer

Francesca Mion<sup>a</sup>, Stefania Vetrano <sup>b,c</sup>, Silvia Tonon<sup>a</sup>, Viviana Valeri<sup>a</sup>, Andrea Piontini <sup>c</sup>, Alessia Burocchi <sup>d</sup>, Luciana Petti<sup>e</sup>, Barbara Frossi <sup>a</sup>, Alessandro Gulino<sup>f</sup>, Claudio Tripodo <sup>f</sup>, Mario P. Colombo <sup>d</sup>, and Carlo E. Pucillo <sup>a</sup>

<sup>a</sup>Department of Medicine, University of Udine, Udine, Italy; <sup>b</sup>Inflammatory Bowel Disease Center, Humanitas Research Hospital, Rozzano, Italy; <sup>c</sup>Department of Biomedical Sciences, Humanitas University, Milano, Italy; <sup>d</sup>Department of Experimental Oncology and Molecular Medicine, Molecular Immunology Unit, Fondazione IRCCS Istituto Nazionale Tumori, Milano, Italy; <sup>e</sup>Department of Biotechnology and Translational Medicine, University of Milan, Milan, Italy; <sup>f</sup>Department of Health Science, Tumor Immunology Unit, Human Pathology Section, Palermo University School of Medicine, Palermo, Italy

### ABSTRACT

One of the most fascinating aspects of the immune system is its dynamism, meant as the ability to change and readapt according to the organism needs. Following an insult, we assist to the spontaneous organization of different immune cells which cooperate, locally and at distance, to build up an appropriate response. Throughout tumor progression, adaptations within the systemic tumor environment, or macroenvironment, result in the promotion of tumor growth, tumor invasion and metastasis to distal organs, but also to dramatic changes in the activity and composition of the immune system. In this work, we show the changes of the B-cell arm of the immune system following tumor progression in the *Apc<sup>Min/+</sup>* model of colorectal cancer. Tumor macroenvironment leads to an increased proportion of total and IL-10-competent B cells in draining LNs while activates a differentiation route that leads to the expansion of IgA<sup>+</sup> lymphocytes in the spleen and peritoneum. Importantly, serum IgA levels were significantly higher in *Apc<sup>Min/+</sup>* than Wt mice. The peculiar involvement of IgA response in the adenomatous transformation had correlates in the gut-mucosal compartment where IgA-positive elements increased from normal mucosa to areas of low grade dysplasia while decreasing upon overt carcinomatous transformation. Altogether, our findings provide a snapshot of the tumor education of B lymphocytes in the *Apc<sup>Min/+</sup>* model of colorectal cancer. Understanding how tumor macroenvironment affects the differentiation, function and distribution of B lymphocytes is pivotal to the generation of specific therapies, targeted to switching B cells to an anti-, rather than pro-, tumoral phenotype.

### ARTICLE HISTORY

Received 6 January 2017  
Revised 25 May 2017  
Accepted 26 May 2017

### KEYWORDS

*Apc<sup>Min/+</sup>* mice; B lymphocytes; IgA; IL-10; intestinal cancer

## Introduction

Colorectal cancer (CRC) is one of the most common malignancies in the world and, despite the significant improvements in screening and treatments, it remains one of the leading causes of tumor-related mortality.<sup>1</sup> As for other types of tumor, immunotherapy represents a fundamental field of study in CRC research.<sup>2</sup> It is now established that the immune system plays a critical role in the development and progression of this type of cancer and that a better understanding of the crosstalk between tumor and immune system is required to overcome immunosuppression and tumor escape.<sup>3,4</sup> Great effort has been devoted to address this issue in the context of the tumor microenvironment (TME). However, tumors release factors and create networks even with distal compartments, leading to the generation of the so-called tumor macroenvironment<sup>5</sup> which should also be considered to understand the crosstalk between CRC and the immune system, and therefore to administer effective immunotherapy.

For many immune cell types it is nowadays possible to define a precise and specific role in the context of the direct or indirect interaction with the tumor, however the same cannot

be said for the B cell arm of the immune system. Indeed, in recent years the contribution of B lymphocytes to tumor immunology turned out to be complex and debated since both pro-tumorigenic and anti-tumor effects have been reported.<sup>6-8</sup> Rosenblatt's group demonstrated that T cell-mediated immune response to primary tumors was stronger in mice genetically lacking B lymphocytes and that high frequencies of intratumoral B cells were associated with increased recruitment and proliferation of regulatory T cells within the tumor microenvironment.<sup>9-11</sup> Conversely, CD20 emerged as new positive prognostic factor in high-grade serous ovarian cancer.<sup>12</sup> These examples of "Janus" B cells are consequences of the inherent complexity of the B cell population.

Traditionally B lymphocytes were described as positive regulators of the immune response due to their fundamental role in humoral immunity and to their capacity to drive T cell activation through antigen presentation, co-stimulation and cytokine production.<sup>13</sup> However, this scenario has become more complex and fascinating following the finding that B cells could also be suppressive and, nowadays, phenotypically diverse B cell populations with regulatory functions have been described in diverse

autoimmune and inflammatory settings.<sup>14</sup> An increasing number of inhibitory mechanisms have been attributed to regulatory B cells (Bregs) although the production of the immunosuppressive cytokine interleukin (IL)-10 remains the most studied.<sup>15</sup>

Most of the literature concerning B cells and CRC focuses on the TME. In patients with CRC, tumor-associated B cells were shown to be enriched for activated and terminally differentiated B cells<sup>16</sup> and Berntsson and coworkers assessed the prognostic impact of tumor-infiltrating B cells and plasma cells (PCs) in CRC.<sup>17</sup> However, since B cell differentiation is strictly related to the specific immunological context, an important aspect that needs further investigation is the understanding of how tumor onset and progression affects B cell biology at the level of the tumor macroenvironment.

Aim of this work was to analyze the tumor-mediated education of B lymphocytes, not only locally, but especially at the systemic level, in the *Apc*<sup>Min/+</sup> model of CRC. The *Apc*<sup>Min/+</sup> mouse is characterized by a mutation in the gene adenomatous polyposis coli (*Apc*) and presents a predisposition to multiple intestinal neoplasia (Min), as such it is widely used as a model for familial adenomatous polyposis (FAP) and for the study of early-stage intestinal tumorigenesis.<sup>18</sup> Our data demonstrate that the frequency and distribution of both B lymphocytes and IL-10-competent B cells is differently affected depending on the specific anatomic site. Specifically, the IL-10-competent B cell population was enlarged in the lymph nodes (LNs) of *Apc*<sup>Min/+</sup> mice while an opposite result was observed in the spleen where a shift toward IgA-secreting PCs steals the show. This study sheds new light on the B cell differentiation processes that occur in the *Apc*<sup>Min/+</sup> model of CRC following tumor onset and progression, and opens a prospect on the specific targeting of B cell subsets for immunological therapies.

## Results

### **Tumor onset in *Apc*<sup>Min/+</sup> mice is associated with a generalized alteration of B cell proportions in peripheral lymphoid organs**

To understand how the tumor macroenvironment affects B cell biology we focused on the *Apc*<sup>Min/+</sup> model of CRC that, beyond resembling human FAP, represents a perfect setting for the analysis of how a developing tumor shapes its environment.<sup>19,20</sup> Specifically, the distribution of B lymphocytes was analyzed in the spleen, peritoneum, mesenteric and inguinal LNs of 18-weeks old animals. At this stage, *Apc*<sup>Min/+</sup> mice of our colonies had multiple intestinal adenomas (Fig. 1A), but did not present signs of exacerbated disease such as severe anemia, rectal prolapse or intestinal occlusion.<sup>21</sup> Dual cell staining with an anti-CD19 mAb and the Live/Dead dye revealed that the frequencies of viable B cells were similar in inguinal LNs of wild-type (Wt) and *Apc*<sup>Min/+</sup> mice, but significantly increased in *Apc*<sup>Min/+</sup> mesenteric LNs, directly draining the tumor site (Figs. 1B and 1C, lower panels). Despite a marked increase in the total number of splenocytes (Fig. S1A), a significant decrease of the percentages of viable CD19<sup>+</sup> cells was detected in the spleen of *Apc*<sup>Min/+</sup> mice compared with the Wt counterpart, and the same result was observed in the peritoneum (Figs. 1B and 1C, upper panels).

The *Apc* tumor suppressor gene plays a key role in the transduction of the Wnt-signaling pathway and it has been demonstrated that the defective Wnt signaling characterizing *Apc*<sup>Min/+</sup> mice influences the development and differentiation of several tissues, including haematopoietic tissues.<sup>22,23</sup> To exclude that the mutation *per se* might be sufficient to explain the altered B cell distribution observed in 18-weeks old *Apc*<sup>Min/+</sup> mice, the frequencies of viable CD19<sup>+</sup> cells were analyzed also in 10-weeks old mice which present few or no macroscopically visible adenomas (Fig. S1B) and an almost regular cellularity of the spleen (Fig. S1C). As shown in Fig. 1C, all organs examined in *Apc*<sup>Min/+</sup> mice at 10 weeks of age did not significantly differ in the percentages of viable B cells compared with the Wt counterpart, indicating that tumor burden is involved in the decrease of B cell frequencies in systemic tissues and in the opposite increase detected in mesenteric draining LNs (dLNs).

In light of these results, we evaluated whether the described findings were peculiar of this mutation-induced setting or common to other consolidated CRC models. To this aim, the percentages of viable CD19<sup>+</sup> cells were compared between healthy controls and mice bearing colitis-associated CRC induced by azoxymethane/dextran sodium sulfate (AOM/DSS), and mice implanted subcutaneously with the CT-26 cell line. Interestingly, although the frequencies of viable B cells were not significantly altered in the spleen and peritoneum of both these 2 models (Fig. 1D, upper panels), these percentages were remarkably higher in inguinal tumor dLNs than in contralateral non-draining LNs (ndLNs) in the case of the transplanted CT-26 model, and in mesenteric dLNs, but not in inguinal ndLNs, of the AOM/DSS setting (Fig. 1D, lower panels).

The finding that the higher B cell proportion in tumor dLNs is common to all the 3 models led us to investigate whether this outcome was the result of an increase in B cell proliferation or of a preferential homing to this lymphoid tissue. The analysis of the B cells staining positive for the nuclear antigen Ki-67 showed that an augmented proliferation rate of this population was not the explanation of the higher percentage of viable CD19<sup>+</sup> cells detected in mesenteric LNs of *Apc*<sup>Min/+</sup> versus Wt mice, since no significant differences were observed (Fig. 1E). Moreover, the percentages of CD19<sup>+</sup>Ki-67<sup>+</sup> cells in ndLNs and dLNs were similar in control and CT-26-bearing mice (Fig. S2A). However, the comparison of Wt and *Apc*<sup>Min/+</sup> mesenteric LNs showed that tumor-bearing mice had a significantly higher expression of CXCL12 and a trend toward a higher expression of CXCL13, CCL19, CCL21 and CCL20, which are all involved in the physiologic homing of lymphocytes to secondary lymphoid organs (Fig. 1F). Interestingly, a similar result was obtained when comparing ndLNs and dLNs from control and CT-26-bearing mice (Fig. S2B). These results indicate that the generation of a lymph node environment that favors B cell recruitment could be the explanation for the higher percentages of B cells detected in dLNs of tumor-bearing mice.

### **Opposite effect of *Apc*<sup>Min/+</sup>-induced intestinal tumorigenesis on the IL-10-competent B cell population of the spleen and LNs**

B cells exerting regulatory suppressive functions through IL-10 secretion have been described in different models of

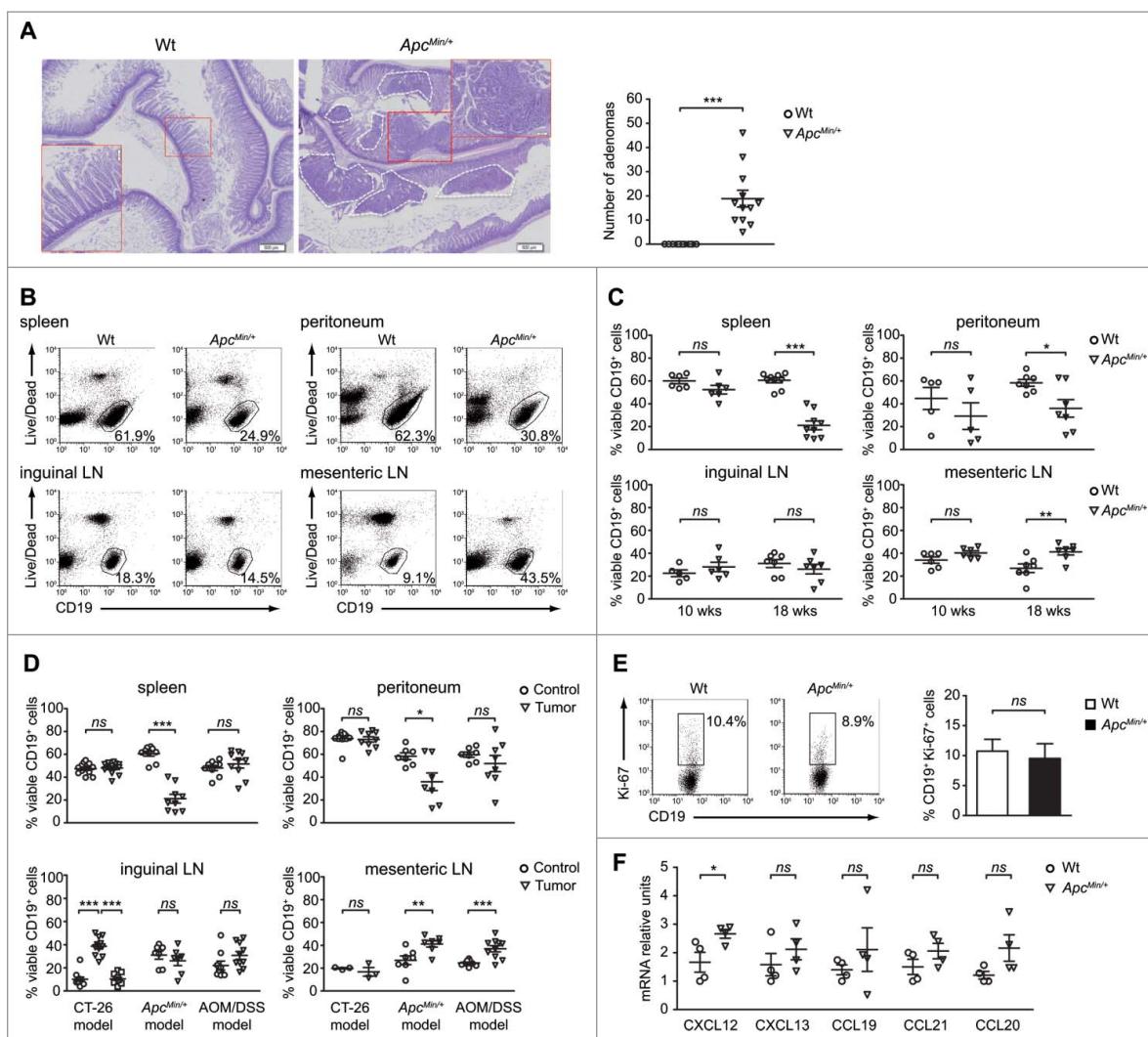


**Figure 1.** B lymphocytes are expanded in tumor-draining LNs of  $Apc^{Min/+}$  mice. (A) Representative pictures of hematoxylin/eosin-stained intestine sections of 18-week old Wt and  $Apc^{Min/+}$  mice (left) and histological scoring of intestinal adenomas (right). Each symbol of the scatter plot depicts individual mice ( $n = 12$ ) among the Wt and  $Apc^{Min/+}$  groups. (B, D) Percentages of viable B cells were analyzed among leukocytes isolated from the spleen, peritoneum, inguinal and mesenteric LNs. In all conditions, cells were treated with LPIM for 5 h before staining. A flow cytometric analysis based on the dual staining with an anti-CD19 mAb and the green Live/Dead probe was performed. (B) B cell frequencies were compared in 18-weeks old Wt and  $Apc^{Min/+}$  mice. Dot plots for one representative experiment are shown. The CD19 vs. Live/Dead plot allows to identify viable B cells (gated) and excludes both non-B cells, which are negative for CD19 staining, and dead cells, that are positively stained with the Live/Dead probe. (C) B cell frequencies were evaluated in 10- and 18-weeks old animals. Each symbol depicts individual mice among the Wt and  $Apc^{Min/+}$  groups (at least  $n = 5$ ) while horizontal lines indicate the mean value  $\pm$  SEM. (D) B cell frequencies were evaluated in the CT-26,  $Apc^{Min/+}$  and AOM/DSS models of CRC. Each symbol depicts individual mice among the control and tumor-bearing group (at least  $n = 3$ ). In the CT-26 model, inguinal LNs were analyzed as draining (triangle symbol) and non-draining (square symbol) the tumor site. Horizontal lines indicate the mean value  $\pm$  SEM. (E) Cells were isolated from mesenteric LNs of 18-weeks old Wt and  $Apc^{Min/+}$  mice and directly underwent the staining procedure for Ki-67 detection. Percentages of Ki-67<sup>+</sup> cells were calculated among viable CD19<sup>+</sup> cells. A representative dot plot and bar graphs reporting the mean values ( $\pm$  SEM) of 3 independent experiments are shown. (F) Relative expression of *cxcl12*, *cxcl13*, *ccl19*, *ccl21* and *ccl20*, normalized to the housekeeping gene *g3pdh*, was analyzed in the total cellular population isolated from the mesenteric LNs of Wt and  $Apc^{Min/+}$  mice ( $n = 4$ ). For each chemokine, the Wt sample with the lowest expression was used as control and set to one. \* $p < 0.05$ ; \*\* $p < 0.01$ ; \*\*\* $p < 0.001$ ; ns: not significant.

autoimmune disease, chronic inflammation and cancer.<sup>24</sup> Given the growing importance of this population, we investigated whether the differentiation of the IL-10-competent B cell population was affected by tumor progression in the  $Apc^{Min/+}$  mouse. After stimulation with LPS, PMA, ionomycin and monensin (LPIM) for 5 h,<sup>25</sup> the percentages of CD19<sup>+</sup>IL-10<sup>+</sup> cells were analyzed among total B lymphocytes of the spleen, peritoneum, mesenteric and inguinal LNs of 18-weeks old  $Apc^{Min/+}$  mice, in comparison to the Wt counterparts. In the peritoneum, the population of IL-10-competent B cells was unaffected by the microenvironment alterations occurring in the  $Apc^{Min/+}$  model. On the contrary, both splenic and LN IL-10-competent B cells were

particularly sensitive to these changes since the percentages of CD19<sup>+</sup>IL-10<sup>+</sup> cells were respectively decreased and increased in  $Apc^{Min/+}$  vs. Wt mice (Fig. 2A). These differences reached statistical significance and were not observed when comparing 10-weeks old animals (Fig. 2B), indicating that the changes in the IL-10-competent B cell population occur when intestinal tumors are fully developed.

Since the differentiation route that leads to the generation of IL-10-competent B cells is strictly environment dependent,<sup>26</sup> we compared the CD19<sup>+</sup>IL-10<sup>+</sup> population in control and tumor-bearing mice also in the CT-26 and AOM/DSS models. Interestingly, this analysis revealed that the alteration of the IL-10-competent B cell profile in



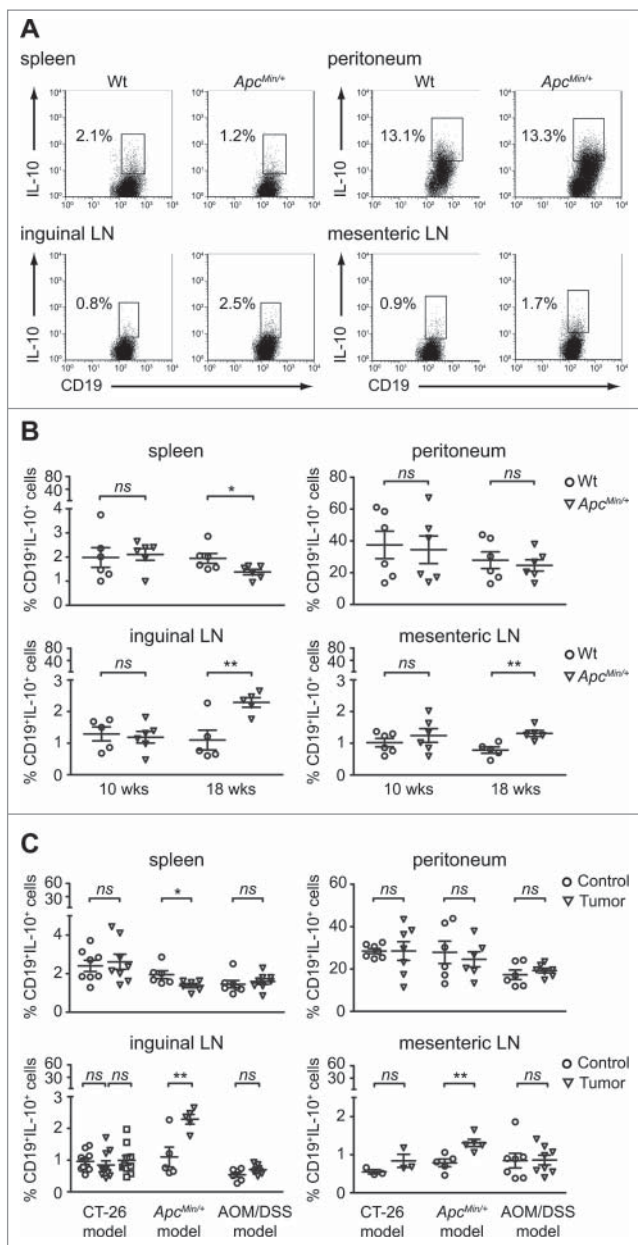


**Figure 2.** Tumor progression leads to discrete alterations of IL-10-competent B cell homeostasis in the  $Apc^{Min/+}$  model of CRC. Percentages of IL-10-competent B cells were analyzed among leukocytes isolated from the spleen, peritoneum, inguinal and mesenteric LNs. In all conditions, cells were treated with LPIM for 5 h before staining with the green Live/Dead probe and the anti-mouse CD19 and anti-mouse IL-10 mAbs. (A) Dot plots from one representative experiment show frequencies of IL-10<sup>+</sup> cells among total viable B cells within the indicated gates in 18-weeks old Wt and  $Apc^{Min/+}$  animals. Dead cells were excluded from the analysis using the CD19 vs. Live/Dead dot plot (data not shown). (B) The IL-10-competent B cell frequencies were evaluated in 10- and 18-weeks old animals. Each symbol depicts individual mice among the Wt and  $Apc^{Min/+}$  groups (at least  $n = 5$ ) while horizontal lines indicate the mean value  $\pm$  SEM. (C) The IL-10-competent B cell frequencies were evaluated in the CT-26,  $Apc^{Min/+}$  and AOM/DSS models of CRC. Each symbol depicts individual mice among the control and tumor-bearing group (at least  $n = 3$ ). In the CT-26 model, inguinal LNs were analyzed as draining (triangle symbol) and non-draining (square symbol) the tumor site. Horizontal lines indicate the mean value  $\pm$  SEM. \* $p < 0.05$ ; \*\* $p < 0.01$ ; ns: not significant.

tumor-bearing mice was peculiar of the  $Apc^{Min/+}$  model. Indeed, in both the CT-26 and in the AOM/DSS settings the rates of CD19<sup>+</sup>IL-10<sup>+</sup> cells were comparable between healthy and tumor-bearing mice in all the anatomic compartments analyzed (Fig. 2C).

### Wt and $Apc^{Min/+}$ B cells are equally competent in responding to activating stimuli

A recent paper published by Ganti and coworkers reported a preferential accumulation of transitional 2-marginal zone precursor (T2-MZP) Bregs in tumor dLNs of mice bearing B16-F10 melanomas. This result was explained by the authors as a mechanism put in place by the tumor itself, which signals *via* the lymphatic drainage to induce an immunosuppressive environment.<sup>27</sup> Similarly, the increased frequencies of CD19<sup>+</sup>IL-10<sup>+</sup> cells detected in dLNs of  $Apc^{Min/+}$  mice might be interpreted as functional to tumor immune escape.

Conversely, the defect in splenic IL-10-competent B cell percentages needed further investigation. We first considered the possibility that Wt and  $Apc^{Min/+}$  B cells could respond differently to classical activation stimuli that we and others have previously demonstrated being involved in B-cell IL-10 competence and production.<sup>25,28</sup> B lymphocytes isolated from the spleen were cultured in medium alone or with agonistic anti-CD40 mAb, LPS or CpG and analyzed for cell proliferation and survival. CFSE dilution assay did not show any relevant difference between Wt and  $Apc^{Min/+}$  B cells (Fig. 3A). Similarly, the viability of untreated and stimulated B cells after 48 h of culture was comparable in the 2 conditions as determined by staining with annexin V and propidium iodide (Table S1). Stimulation through CD40 is required for the development, maturation, and/or expansion of IL-10-competent B cells while TLR agonists are necessary for the production and secretion of this cytokine.<sup>25,28,29</sup> Interestingly, splenic Wt and  $Apc^{Min/+}$  B cells responded similarly to stimulation in terms of IL-10 competence and production. Indeed, an average percentage of CD19<sup>+</sup>IL-10<sup>+</sup> cells of about 5% was detected in both conditions after 48 h of stimulation with the agonistic anti-CD40 mAb (Fig. 3B) and the amounts of IL-10 secreted upon LPS or CpG treatment were significantly increased in respect of untreated B cells, but did not differ among the Wt and  $Apc^{Min/+}$  conditions (Fig. 3C, left panel). In addition to IL-10, the production of the regulatory marker latency-associated peptide-1 (LAP-1) was analyzed. Again, a very similar trend in terms of response to stimulation was observed between the 2 conditions, although B cells isolated from the spleen of  $Apc^{Min/+}$  mice presented a higher basal release of this cytokine compared with Wt B cells (Fig. 3C, right panel). Altogether these data demonstrate that a different response to classical B cell stimuli is not underlie the lower percentage of IL-10-competent B cells observed in the spleen of  $Apc^{Min/+}$  mice.

### Increasing age and adenoma burden lead to a marked alteration of the B cell proportions among the phenotypical subsets of the spleen

We subsequently investigated another possible explanation of the reduced frequency of splenic IL-10-competent B cells that implied a different B cell distribution among the functional and phenotypical compartments of the spleen. Based on the differential expression of the CD21 and CD23 surface markers, splenic B lymphocytes can be subdivided into at least 3 main populations, namely the newly formed (NF), marginal zone (MZ) and follicular (FO) B cell subsets. Three-color CD19/

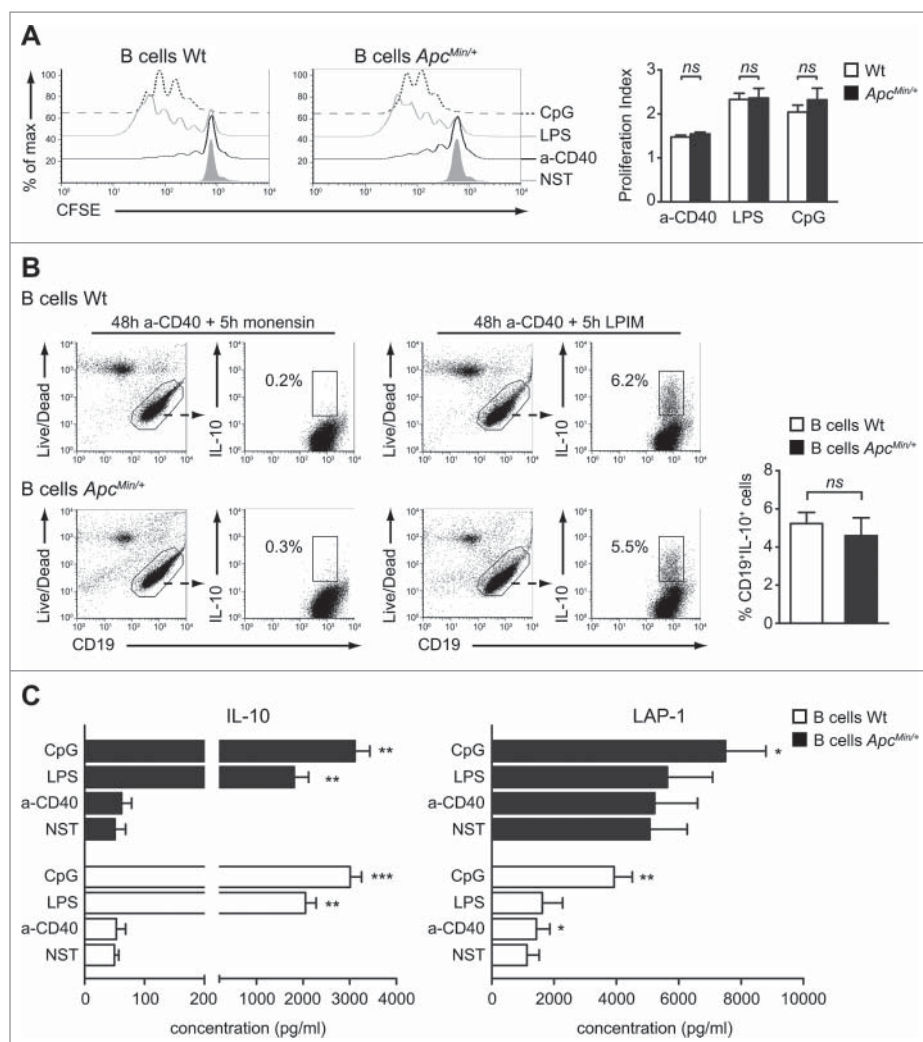


**Figure 3.** Wt and *Apc<sup>Min/+</sup>* splenic B cells respond similarly to activating stimuli. (A) B cells were purified from the spleen of Wt and *Apc<sup>Min/+</sup>* mice, CFSE labeled and cultured either alone (NST) or in the presence of anti-CD40 mAb (a-CD40), LPS or CpG for 72 h. CFSE profiles of B cell proliferation in the different conditions are shown for one representative experiment while bar graphs indicate mean (+ SEM) of the B cell proliferation index from 5 independent experiments. (B) The frequencies of B cells competent to express cytoplasmic IL-10 following a 5 h stimulation with LPIM were analyzed in purified Wt and *Apc<sup>Min/+</sup>* B cells cultured for 48 h with anti-CD40 mAb. The condition in which cells received only monensin during the last 5 h of culture was used to correctly discriminate IL-10<sup>+</sup> from IL-10<sup>-</sup> B cells. Dot plots for one representative experiment are shown together with the frequencies of IL-10<sup>+</sup> cells among total CD19<sup>+</sup> lymphocytes. Bar graphs indicate mean (+ SEM) percentages of CD19<sup>+</sup>IL-10<sup>+</sup> cells from 6 independent experiments. (C) B cells were cultured either alone (NST) or in the presence of a-CD40 mAb, LPS or CpG for 48 h. Cell supernatants were collected and IL-10 and LAP-1 levels detected by ELISA. Bar graphs indicate mean (+ SEM) concentrations from 6 independent experiments and comparison were performed against the NST condition. \**p* < 0.05; \*\**p* < 0.01; \*\*\**p* < 0.001; ns: not significant.

CD21/CD23 flow cytometry analyses of Wt and *Apc<sup>Min/+</sup>* splenocytes revealed a completely altered distribution of *Apc<sup>Min/+</sup>* B cells which were present in lower percentages among the FO and MZ compartments (Fig. 4A). The decrease of B lymphocytes with a MZ phenotype was confirmed by the triple immunofluorescence staining with Abs against the CD19, CD1d and CD5 molecules. High expression levels of CD1d is a peculiar feature of MZ B cells<sup>30</sup> and, as shown in Fig. 4B, CD19<sup>+</sup> cells with a CD1d<sup>hi</sup> phenotype were reduced in percentage in *Apc<sup>Min/+</sup>* compared with Wt mice. Moreover, this second type of staining evidenced a significant reduction also in the percentage of CD1d<sup>+</sup>CD5<sup>+</sup> B10 cells which, together with MZ and T2-MZP B cells, represent a compelling candidate for the regulatory activity of B lymphocytes.<sup>31</sup> If on one hand the phenotypic analyses of *Apc<sup>Min/+</sup>* B lymphocytes evidenced a reduced percentage of B cells with Breg traits, on the other the CD21/CD23 staining revealed a statistically significant enlargement of

the compartments characterized by low/negative levels of the CD21 receptor (Fig. 4A). Similarly to what observed for the IL-10-competent B cell analysis (Fig. 2), the altered B cell distribution among the phenotypic subsets was detected when comparing 18- but not 10-weeks old Wt and *Apc<sup>Min/+</sup>* mice (Figs. 4C and S3A) and was not paralleled neither in the AOM/DSS nor in the CT-26 model of CRC (Figs. S3B and S3C). Therefore, the described changes are peculiar of the mutation-induced model of CRC, but tumor onset is required for the manifestation of the phenotype.

#### *Apc<sup>Min/+</sup>* mice present traits of a skewing toward IgA-producing cells

Deepening into the characterization of these *Apc<sup>Min/+</sup>* CD21<sup>low</sup> cells, we observed phenotypic similarities with a small subset of CD19<sup>+</sup>CD45R<sup>low/-</sup>CD21<sup>low</sup> lymphocytes that was recently

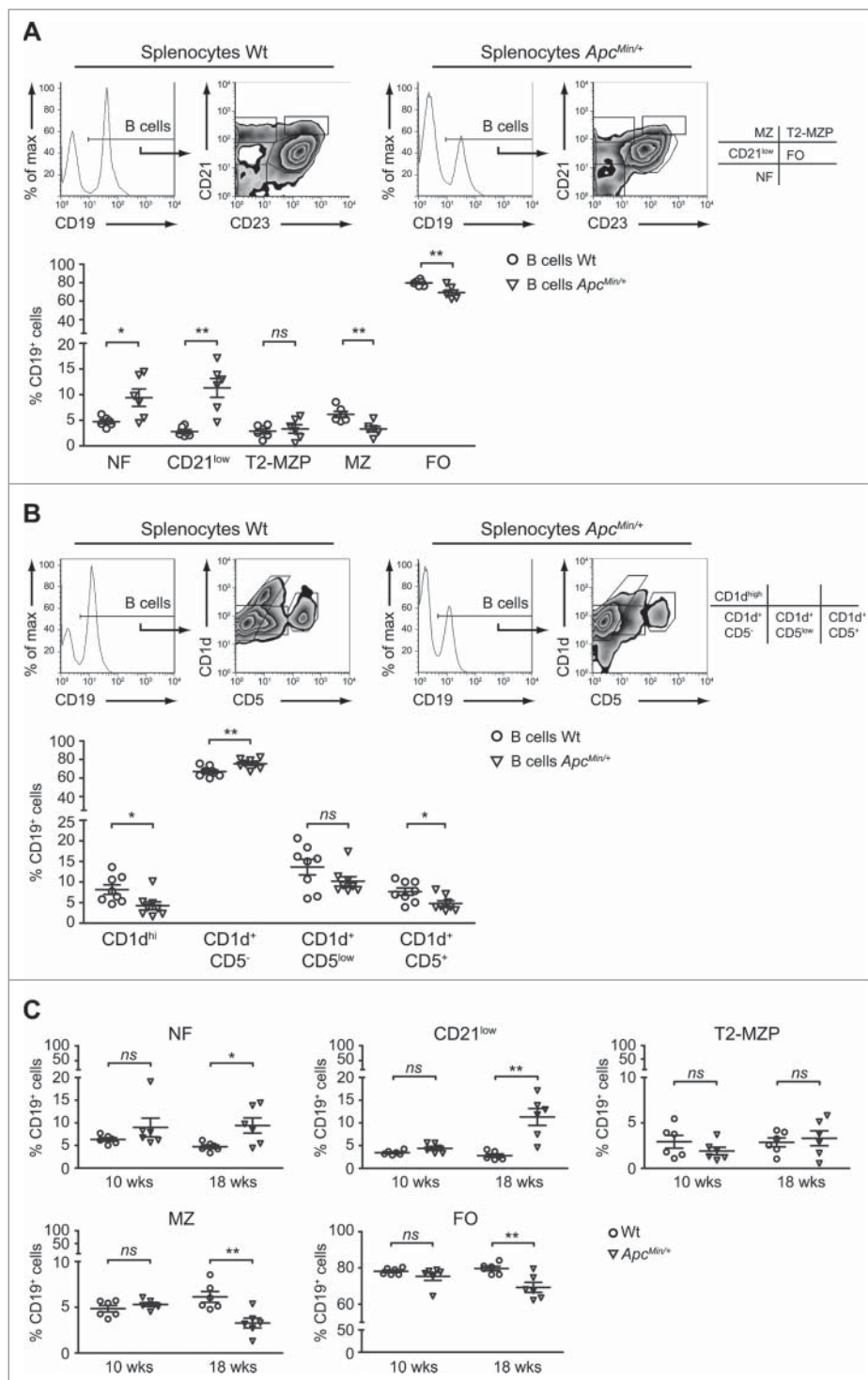


**Figure 4.** B cells with a CD21<sup>low</sup> phenotype are enriched in the spleen of tumor-bearing *Apc<sup>Min/+</sup>* mice. Splenocytes were isolated from 18-weeks old Wt and *Apc<sup>Min/+</sup>* mice, stained with anti-CD21, -CD23 and -CD19 (A, C) or with anti-CD1d, -CD5, and -CD19 (B) mAbs and analyzed by flow cytometry. (A, B) Histogram and dot plots show the analysis of one representative mouse *per* condition while scatter plots report the mean ( $\pm$  SEM) percentages of CD19<sup>+</sup> cells with the phenotype of newly formed (NF), CD21<sup>low</sup>, transitional 2-marginal zone precursor (T2-MZP), marginal zone (MZ) and follicular (FO) cells (A) or of CD1d<sup>hi</sup>, CD1d<sup>+</sup>CD5<sup>-</sup>, CD1d<sup>+</sup>CD5<sup>low</sup> and CD1d<sup>+</sup>CD5<sup>+</sup> cells (B). Each symbol depicts individual mice among the Wt and *Apc<sup>Min/+</sup>* groups ( $n = 6$  in A;  $n = 8$  in B). (C) The percentages of CD19<sup>+</sup> cells with a NF, CD21<sup>low</sup>, T2-MZP, MZ and FO phenotype were analyzed in 10- and 18-weeks old Wt and *Apc<sup>Min/+</sup>* mice ( $n = 6$ ). \* $p < 0.05$ ; \*\* $p < 0.01$ ; *ns*: not significant.

described in the spleen of adult mice and that is enriched in natural PCs spontaneously secreting IgG and IgA.<sup>32,33</sup> In fact, the expression of the surface markers CD45R and CD138 resulted respectively down- and up-modulated on CD21<sup>low</sup> compared with FO and MZ cells (Fig. 5A). These phenotypic similarities raised our interest in understanding whether the

expansion of CD21<sup>low</sup> B cells was a free-standing event, or rather the result of a tumor macroenvironment-induced differentiation process aimed at expanding the final mediators of the humoral response.

In this view, we first evaluated whether the CD19<sup>+</sup>CD45R<sup>low</sup> population was preferentially found in the



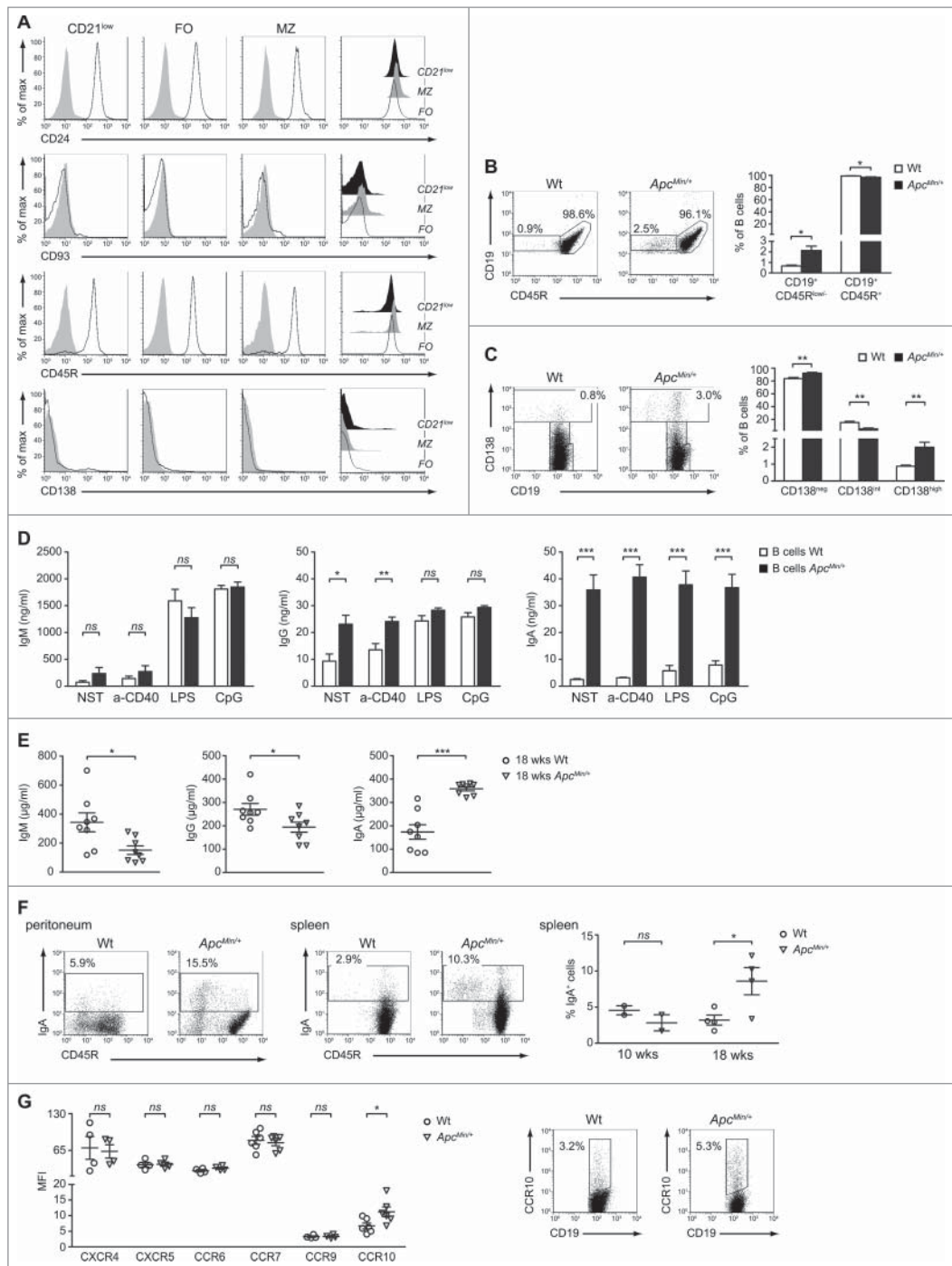


**Figure 5.** Tumor progression induces a strong IgA response in *Apc*<sup>Min/+</sup> mice. (A) Representative analysis of CD24, CD93, CD45R and CD138 expression on CD21<sup>low</sup>, FO and MZ B cells from the spleen of 18-weeks old *Apc*<sup>Min/+</sup> mice. Single-color histograms are plotted against log fluorescence intensity of the specific Ag are the result of a 4-color staining. Filled and empty histograms indicate isotype-matched controls and specific Abs, respectively. For each of the 4 phenotypic markers in analysis, a plot overlaying the expression patterns among the CD21<sup>low</sup>, FO and MZ populations is shown on the right. (B) Representative dot plots showing the CD19<sup>+</sup>CD45R<sup>+</sup> and CD19<sup>+</sup>CD45R<sup>low/-</sup> subsets in Wt and *Apc*<sup>Min/+</sup> mice. Non-B cells were excluded from the analysis. Bar graphs indicate mean (+ SEM) percentages of CD19<sup>+</sup>CD45R<sup>+</sup> and CD19<sup>+</sup>CD45R<sup>low/-</sup> cells among total B lymphocytes from 4 independent experiments. (C) Representative dot plots showing the CD138<sup>neg</sup>, CD138<sup>int</sup> and CD138<sup>high</sup> subsets in Wt and *Apc*<sup>Min/+</sup> mice. Non-B cells were excluded from the analysis. Bar graphs indicate mean (+ SEM) percentages of CD138<sup>neg</sup>, CD138<sup>int</sup> and CD138<sup>high</sup> cells among total B lymphocytes from 6 independent experiments. (D) B cells were cultured either alone (NST) or in the presence of a-CD40 mAb, LPS or CpG for 48 h. Cell supernatants were collected and IgM, IgG and IgA levels detected by ELISA. Bar graphs indicate mean (+ SEM) concentrations from 4 to 6 independent experiments. (E) Total IgM, IgG and IgA were measured by ELISA in the serum of 18-weeks old Wt and *Apc*<sup>Min/+</sup> mice (n = 8). (F) B cells purified from the peritoneum and spleen of 18-weeks old Wt and *Apc*<sup>Min/+</sup> mice were stained for CD45R and IgA and analyzed by flow cytometry. Dot plots are shown together with the percentages of IgA<sup>+</sup> cells and are representative of n = 2 (peritoneum) and n = 4 (spleen) experiments. Non-B cells were excluded from the analysis. The scatter plot reported on the right is the result of the analysis of IgA<sup>+</sup> cells in the spleen of 10- and 18-weeks old Wt and *Apc*<sup>Min/+</sup> mice. (G) Wt and *Apc*<sup>Min/+</sup> splenocytes were stained for CD19 and CXCR4, CXCR5, CCR6, CCR7, CCR9 or CCR10. The scatter plot reports the mean fluorescence intensity (MFI) of each chemokine receptor. Each symbol depicts individual mice among the Wt and *Apc*<sup>Min/+</sup> groups (at least n = 4) while horizontal lines indicate the mean value ± SEM. For CCR10, the dot plots of one representative experiment are shown with indicated the percentages of CD19<sup>+</sup>CCR10<sup>+</sup> cells. \*p < 0.05; \*\*p < 0.01; \*\*\*p < 0.001; ns: not significant.

spleen of our mutation-induced model of CRC and what we observed was a statistical significant increase of CD19<sup>+</sup>CD45R<sup>low/-</sup> cell percentages in the *Apc*<sup>Min/+</sup> compared with the Wt condition (Fig. 5B). The switch toward a PC phenotype in *Apc*<sup>Min/+</sup> mice was confirmed by analyzing the expression of the CD19 and CD138 surface molecules. Several studies show that the differential expression of these 2 markers allow to define distinct intermediate stages of PC differentiation.<sup>34</sup> Normal levels of CD19 and intermediate levels of CD138 (CD138<sup>int</sup>) characterize the pre-PC population while high levels of CD138 (CD138<sup>high</sup>) and a gradual down modulation of CD19 are indicative of a shift to a later stage of differentiation, that is the one of PC.<sup>35</sup> Interestingly, the frequency of CD138<sup>high</sup> PCs, calculated among total splenic B lymphocytes, was 2.3-fold higher in *Apc*<sup>Min/+</sup> than Wt mice and this difference reached statistical significance (Fig. 5C). Another evidence strictly associated with the presence of highly differentiated B cells in the spleen of *Apc*<sup>Min/+</sup> mice was obtained by analyzing immunoglobulin concentrations in culture supernatants of untreated and *in vitro*-stimulated B lymphocytes. In fact, in spite of a comparable release of IgM, both under basal conditions and following activation, *Apc*<sup>Min/+</sup> B cells spontaneously produced significantly higher amounts of IgG and IgA compared with Wt B cells (Fig. 5D). Of note, the IgA concentrations detected in the culture medium of untreated *Apc*<sup>Min/+</sup> B cells were 14-fold higher than in Wt B cells and did not reach comparable levels neither under the effect of *in vitro* stimulation, revealing a strong *in vivo* priming of *Apc*<sup>Min/+</sup> B cells toward IgA production. Even more importantly, a comparable increase in immunoglobulin production and IgA skewing was not observed when comparing neither 10-weeks old Wt and *Apc*<sup>Min/+</sup> mice (Fig. S4A) nor healthy and CT-26 tumor-bearing mice (Fig. S4B). In this light, we went ahead and assessed the levels of circulating antibodies. Interestingly, the analysis of IgM, IgG and IgA abundance in mouse sera revealed that, in respect to the Wt counterpart, *Apc*<sup>Min/+</sup> animals had significantly higher concentrations of IgA, but not of IgM and IgG (Fig. 5E). Again, this difference in IgA titers was not observed when comparing 10-weeks old mice (Fig. S4C), suggesting the presence of a correlation between the humoral immune status and tumor progression.

Altogether these results prompted us to assess whether, along with the activation of mechanisms responsible for IgA production, the initiation of this strong IgA response could also be due to enhanced IgA class switching among the *Apc*<sup>Min/+</sup> B cell pool. The analysis of IgA expression at the cellular level confirmed this hypothesis since the frequency of B lymphocytes staining positive for the membrane-bound form of IgA was higher in *Apc*<sup>Min/+</sup> than in control mice, both in the splenic and peritoneal compartments (Fig. 5F). IgA-secreting PCs promptly migrate in response to CCL25 and CCL28, 2 chemokines primarily expressed by mucosal epithelial cells.<sup>36</sup> Importantly, when addressing the expression of lymphocyte-associated chemokine receptors on splenic Wt and *Apc*<sup>Min/+</sup> B cells, we found that CCR10 was the only one to present a statistically significant difference in terms of mean fluorescence intensity (Fig. 5G, left panel). Both the Wt and *Apc*<sup>Min/+</sup> B cell populations were positive for CXCR4, CXCR5, CCR6 and CCR7 while CCR9 and CCR10 were expressed at lower levels.

However, a higher percentage of CD19<sup>+</sup>CCR10<sup>+</sup> cells was detected among *Apc*<sup>Min/+</sup> B lymphocytes (Fig. 5G, right panel), supporting the evidence of an enrichment in IgA-secreting PCs in this mutation-induced model of CRC.

### **B cells produce IgA following co-culture with *Apc*<sup>Min/+</sup>-derived CD11b<sup>+</sup>Gr-1<sup>+</sup> cells**

Our observations showed that developing tumors in *Apc*<sup>Min/+</sup> mice cause a significant alteration of splenic B cell homeostasis, that results in a decreased proportion of IL-10-competent B cells and in the parallel occurrence of IgA-secreting cell traits. The alteration of the splenic micro-environment was not restricted to the B cell compartment since 18-weeks old, but not 10-weeks old, *Apc*<sup>Min/+</sup> mice presented a significantly higher percentage of CD11b<sup>+</sup>Gr-1<sup>+</sup> cells, compared with the Wt counterpart (Figs. 6A and S5A). Although nowadays new biochemical and molecular characteristics have emerged, historically the co-expression of the CD11b and Gr-1 markers broadly defines myeloid-derived suppressor cells (MDSCs), a heterogeneous population of immature granulocytes, macrophages, and dendritic cells which accumulate in large numbers in lymphoid tissues of tumor-bearing mice.<sup>37,38</sup> Since an increasing amount of data demonstrates an association between the large accumulation of MDSCs and the modulation of B cell differentiation and function in infection, autoimmune and tumor settings,<sup>39-41</sup> we decided to assess whether CD11b<sup>+</sup>Gr-1<sup>+</sup> cells took part to the skewing toward IgA-producing cells observed in *Apc*<sup>Min/+</sup> mice.

CD11b<sup>+</sup>Gr-1<sup>+</sup> cells were isolated from the spleen of 18-weeks old *Apc*<sup>Min/+</sup> mice and cultured with age-matched Wt CD19<sup>+</sup> cells at a 1:1 ratio for 48 h, in the presence or absence of LPS (Fig. 6B). Following co-culture, IgA<sup>+</sup> B cells were analyzed by flow cytometry while supernatants were assayed for IgA and IgG by ELISA. As shown in Fig. 6C, the percentages of cells staining positive for membrane-bound IgA were not affected by the presence of CD11b<sup>+</sup>Gr-1<sup>+</sup> cells, suggesting that in our experimental system MDSCs do not provide signals inducing IgA class switching. On the contrary, the interaction with CD11b<sup>+</sup>Gr-1<sup>+</sup> cells significantly influenced the production of soluble IgA since the concentrations detected among B cells cultured alone were about 12 times lower than those detected in the co-culture. When LPS was added to the system, the release of IgA by B cells alone was higher but still 4 times lower compared with the condition in which CD11b<sup>+</sup>Gr-1<sup>+</sup> cells were also present (Fig. 6D). Strengthening the hypothesis of a role played by CD11b<sup>+</sup>Gr-1<sup>+</sup> cells in the enhanced production of IgA detected in our mutation-induced model of CRC, is the result that CD11b<sup>+</sup>Gr-1<sup>+</sup> cells did not have the same effect in respect to IgG production. Indeed, as shown in Fig. 6E, LPS but not MDSCs significantly increased the levels of total IgG released by B lymphocytes. Moreover, a modest increment of IgG concentrations was detected in the B/MDSC co-culture, but only in the absence of LPS stimulation. Altogether these data are suggestive of a relevant role played by CD11b<sup>+</sup>Gr-1<sup>+</sup> cells in the *in vivo* priming received by *Apc*<sup>Min/+</sup> B cells, responsible of the increased production of IgA observed in this mouse model.



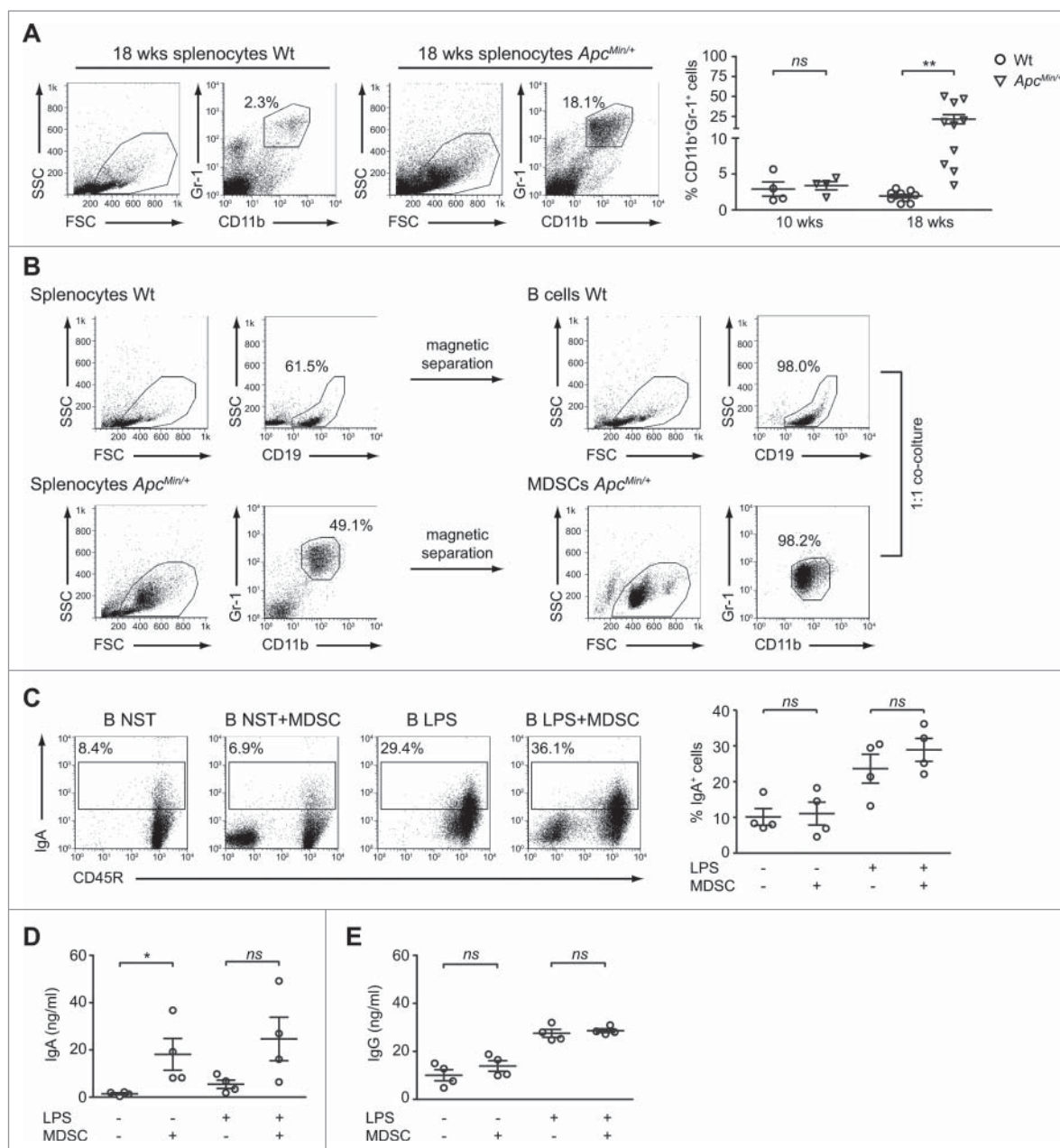


**Figure 6.** *Apc*<sup>Min/+</sup> CD11b<sup>+</sup>Gr-1<sup>+</sup> cells increase the production of IgA by B lymphocytes. (A) Cells were isolated from the spleen of 18-weeks old Wt and *Apc*<sup>Min/+</sup> mice, stained with anti-CD11b and anti-Gr-1 mAbs and analyzed by flow cytometry. Representative dot plots are reported with indicated percentages of double positive cells. The scatter plot shows mean (± SEM) percentages of CD11b<sup>+</sup>Gr-1<sup>+</sup> cells among total Wt and *Apc*<sup>Min/+</sup> splenocytes of both 10- (n = 4) and 18-weeks old (n = 10) mice. (B) Gating strategy for purity check of Wt B cells (upper panels) and *Apc*<sup>Min/+</sup> CD11b<sup>+</sup>Gr-1<sup>+</sup> cells (lower panels) in the pre-isolation and post-isolation steps. (C, D, E) B cells were cultured with CD11b<sup>+</sup>Gr-1<sup>+</sup> cells for 48 h, in the presence or absence of LPS. After co-culture, cells were stained for CD45R and IgA (C) while culture supernatants were assessed by ELISA for the presence of soluble IgA (D) and IgG (E). Dot plots for one representative experiment are shown with indicated percentages of IgA<sup>+</sup> cells among B lymphocytes. Scatter plots indicate mean (± SEM) percentages of IgA<sup>+</sup> cells (C) and mean (± SEM) IgA (D) and IgG (E) concentrations from 4 independent experiments. \**p* < 0.05; \*\**p* < 0.01; *ns*: not significant.

### The local distribution of gut IgA<sup>+</sup> cells is affected in the adenoma-carcinoma sequence

The colorectal adenoma-carcinoma sequence stands for the stepwise process that progresses from normal to dysplastic epithelium to carcinoma, and that is associated with the accumulation of multiple clonally selected genetic alterations.<sup>42</sup> In light of the switch of the systemic B lymphocyte population toward IgA-producing cells, we were finally interested in investigating whether also the homeostasis of local mucosal IgA<sup>+</sup> PCs was affected by tumor progression and if there was a correlation

between the distribution of IgA<sup>+</sup> cells and the adenoma-carcinoma sequence.

Immunohistochemistry was used to examine the IgA-producing B cell population in the small intestine of Wt and *Apc*<sup>Min/+</sup> mice and revealed the absence of a difference in the number of IgA-positive elements between the 2 conditions (Fig. 7A). Nonetheless, the intriguing result of this analysis was the peculiar distribution of these IgA-positive elements in the adenoma tissue compared with the normal mucosa of *Apc*<sup>Min/+</sup> mice. In the undamaged mucosa IgA<sup>+</sup> cells were evenly spread; however, when moving to the areas affected by the lesion, we

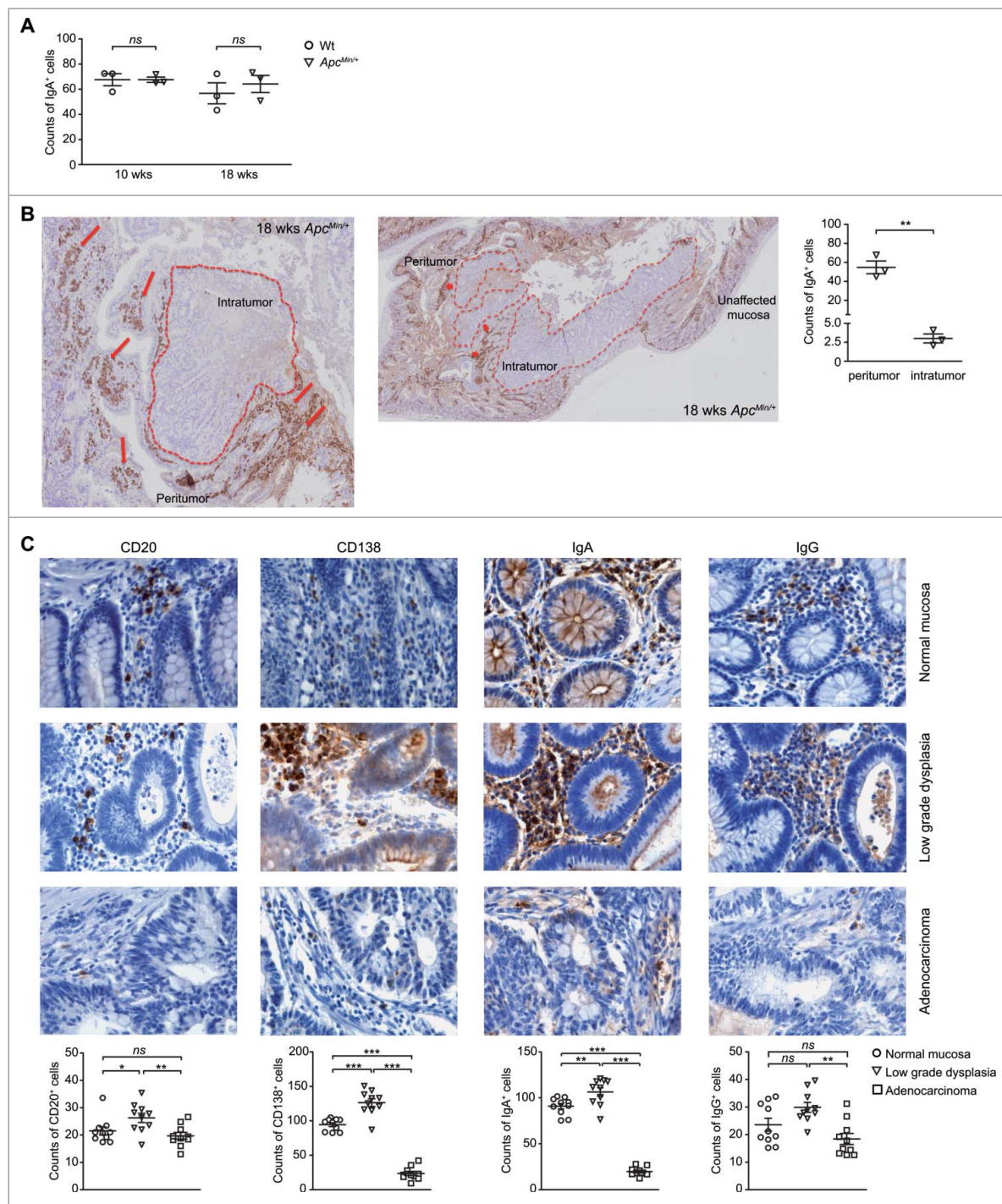


**Figure 7.** IgA-positive elements are extruded from intestinal adenocarcinomas both in the mouse and in humans. (A) Quantification of IgA-positive elements in small intestine sections of 10- and 18-week old animals. Each symbol depicts individual mice among the Wt and *Apc<sup>Min/+</sup>* groups ( $n = 3$ ) while horizontal lines indicate the mean value  $\pm$  SEM. Each symbol of the scatter plot is the mean count of 10 fields (20x). (B) Representative immunohistochemistry analysis of IgA in the small intestine of 18-weeks old *Apc<sup>Min/+</sup>* mice. Normal mucosa shows uniform IgA staining while dysplastic regions show a stronger IgA immunoreactivity. Intratumoral IgA-positive elements were seldomly observed. The comparison of IgA counts within the dysplastic and intratumoral regions are also provided ( $n = 3$ ). Each symbol of the scatter plot is the mean count of 10 fields (20x). (C) Representative immunohistochemistry analysis of anti-CD20, anti-CD138, anti-IgA and anti-IgG immunostaining of formalin-fixed paraffin-embedded intestinal sections of patients affected by CRC. For each human sample, areas of unaffected mucosa, low grade dysplasia and adenocarcinoma were examined. Counts of CD20<sup>+</sup>, CD138<sup>+</sup>, IgA<sup>+</sup> and IgG<sup>+</sup> elements are also provided. Each symbol of the scatter plot is the mean count of 5 fields (40x). Horizontal lines indicate the mean value  $\pm$  SEM. \* $p < 0.05$ ; \*\* $p < 0.01$ ; \*\*\* $p < 0.001$ ; ns: not significant.

clearly observed a high accumulation of IgA-positive elements close to the areas of low grade dysplasia while these cells were almost completely extruded from the adenomas (Fig. 7B).

This result prompted the investigation of whether the observed correlation between the distribution of IgA<sup>+</sup> cells and

the adenoma-carcinoma sequence had a parallel in the human setting. In this view, colon biopsy specimens from 10 patients diagnosed for CRC were analyzed by immunohistochemistry for the presence and distribution of CD20<sup>+</sup>, CD138<sup>+</sup>, IgA<sup>+</sup> and IgG<sup>+</sup> cells in the undamaged mucosa, in areas of low

grade-dysplasia and within the adenocarcinoma. Interestingly, although no major differences were highlighted in the counts of CD20<sup>+</sup> and IgG<sup>+</sup> elements within the lamina propria of normal mucosa and adenocarcinomas, the density of both CD138<sup>+</sup> and IgA<sup>+</sup> cells showed a peculiar inverted U-shaped trend in the colorectal adenoma-carcinoma sequence (Fig. 7C). In fact, anti-IgA and anti-CD138 immunostaining revealed an increased number of CD138<sup>+</sup> and IgA<sup>+</sup> cells in the areas of low grade dysplasia compared with both unaffected mucosa and especially to the invasive adenocarcinoma where these elements were sparsely distributed. Notably, immunofluorescence microscopy analysis showed the co-localization of the PC marker CD138 and IgA (Fig. S6). These results are in accordance with previously published studies,<sup>43,44</sup> which reported a reduced density of CD138<sup>+</sup>IgA<sup>+</sup> cells in the adenocarcinoma-associated compared with the undamaged colonic mucosa. Altogether these results are suggestive of a role of IgA<sup>+</sup> PCs in the early phases of CRC progression.

## Discussion

In the present study, the crosstalk between B lymphocytes and tumor was addressed under a novel perspective. Differently from other works on the topic, our investigation took into analysis the changes in the distribution, phenotype and functions of B lymphocytes during tumor progression and was not limited to the draining LNs and lymphoid structures associated to the TME. Research in the field of tumor immunology is principally focused on deciphering the immune response toward cancer and increasing efforts are directed to the study of the intercellular communication between malignant and non-transformed cells. This TME-centered point of view detract attention from an equally important aspect that is the effect on the immune system of the so-called tumor macroenvironment.<sup>45</sup> As reviewed by Al-Zhoughbi and coworkers, the tumor macroenvironment develops as a slow multi-step process, driven by the release in the blood and/or lymph stream of soluble factors produced by the tumor and its microenvironment. Cancer is a systemic disease and a better understanding of the role of host macroenvironment in tumor progression is of clinical relevance.<sup>46</sup>

With the aim of studying the systemic interactions between the tumor and B lymphocytes in the context of CRC, we considered the *Apc*<sup>Min/+</sup> mouse a suitable model due to the possibility of assessing the changes of the B cell population at different stages of tumor progression. The distribution of B lymphocytes among different organs, together with the analysis of classical markers of the splenic B cell phenotype, demonstrated that the B cell arm of the immune system is significantly affected by tumor progression. The analysis of 10-weeks old animals showed that the B cell situation in *Apc*<sup>Min/+</sup> mice was almost normal compared with the Wt counterpart. Conversely, at 18 weeks of age, when the contribution of the tumor macroenvironment is greater, we observed a considerable decrease of B cell percentages in the spleen, accompanied by a completely altered B cell phenotypic pattern in the splenic compartment. The contribution of tumor macroenvironment was also suggested by Cotella and coworkers as possible explanation for their elegant observation that older, but not younger, *Apc*<sup>Min/+</sup>

mice displayed a decrease in pro-, pre- and immature B cells in the bone marrow.<sup>22</sup> Differently from what observed in the spleen, B lymphocytes were significantly increased in percentage in mesenteric LNs of 18-weeks old *Apc*<sup>Min/+</sup> mice. The enlargement of the B cell population in tumor draining LNs was not specific of the *Apc*<sup>Min/+</sup> mouse but, on the contrary, it appeared to be a generalized mechanism related to tumor onset since it was observed in 2 other models of CRC set up in this study and in other recently published reports.<sup>27,47</sup> The comparison of the *Apc*<sup>Min/+</sup>, CT-26 and AOM/DSS models leads to the obvious question of why the B cell populations of the spleen did not act at the same way in the 3 tumor settings. Although not supported by experimental data, the answer lies in the diversity inherent to the 3 models. The complexity and specific characteristics of the native microenvironment are lost in the ectopic implantation model, while, in the AOM/DSS setting, tumors develop under the environmental influences of chronic inflammation.<sup>48</sup> This could also explain the differences observed when analyzing the percentages of CD19<sup>+</sup>IL-10<sup>+</sup> cells which differed between healthy and tumor-bearing mice in the *Apc*<sup>Min/+</sup> but not in the CT-26 and AOM/DSS models. Indeed, after a first analysis of the B cell population *in toto*, we focused on IL-10-competent Bregs that are riding high in the context of the role of B cells in the TME,<sup>49</sup> but have been broadly analyzed in respect to tumor macroenvironment. Interestingly, as mice grew older and tumor progression advanced, the percentages of CD19<sup>+</sup>IL-10<sup>+</sup> cells increased in LNs but decreased in the spleen of *Apc*<sup>Min/+</sup> mice.

If locally the tumor seems to induce an immunosuppressive environment, systemically several results obtained in this work lead to speculate a switch to IgA-producing PCs. Fueled by the curious and unexpected observation that *Apc*<sup>Min/+</sup> mice upregulated the CD19<sup>+</sup>CD45R<sup>low/-</sup>CD21<sup>low</sup> population, poised for spontaneous secretion of IgA and IgG antibodies,<sup>32,33</sup> we analyzed the sera of both Wt and *Apc*<sup>Min/+</sup> mice and found that total IgA, but not IgM and IgG, levels were significantly higher in tumor-bearing compared with healthy mice. This result finds support, and becomes even more relevant, in light of the evidence that a relation between elevated serum IgA levels and cancer had already been brought to light in the 80s in the context of human tumors of the upper respiratory tract and colon<sup>50</sup> and, more recently, in neoplastic disorders of breast.<sup>51</sup> Our experiments show that higher percentages of IgA-switched B cells are present in the spleen and peritoneum of our genetic model of CRC. In this context, also the greater basal production of LAP-1 by *Apc*<sup>Min/+</sup> B lymphocytes finds a possible explanation. Indeed, it has been shown that CD40 triggering leads to IgA switching through induction of endogenous TGF- $\beta$  and the unleashing of an autocrine TGF- $\beta$ -dependent loop.<sup>52,53</sup> Moreover, the spontaneous release of large amounts of IgA by *Apc*<sup>Min/+</sup> B cells is suggestive of a strong *in vivo*, tumor macroenvironment-induced, priming toward IgA production.

Since Wt and *Apc*<sup>Min/+</sup> B cells responded very similarly to the classical activating stimuli, we tested the hypothesis that the phenotypical and functional changes of the splenic B cell population were the consequences of a change in the nature of the received signals. An increase in the frequency of CD11b<sup>+</sup>Gr-1<sup>+</sup> MDSCs was reported to be a trait of tumor progression in several mouse tumor models and clinical studies.<sup>54</sup> Here we show



that CD11b<sup>+</sup>Gr-1<sup>+</sup> cells are expanded in the spleen of our genetic model of CRC. *Apc*<sup>Min/+</sup> MDSCs alone might play a relevant role in the *in vivo* priming of *Apc*<sup>Min/+</sup> B cells toward IgA production while they might require the cooperation of other tumor macroenvironment-derived signals to power the differentiation processes leading to the expansion of the final mediators of the humoral response. These considerations derive from our *in vitro* experiments showing that *Apc*<sup>Min/+</sup> CD11b<sup>+</sup>Gr-1<sup>+</sup> cells are able to induce the production of IgA but not the expansion of CD138<sup>high</sup> PCs (data not shown) nor of IgA-switched B cells. Although the literature regarding the B cell/MDSC crosstalk is quite diverse and dependent on the specific context analyzed, our results are in line with a recently published work reporting that, when *in vitro* cultured with non-adherent spleen cells, MDSCs promote both proliferation and differentiation of B cells into IgA-producing PCs.<sup>41</sup>

The gut mucosa is the site *par excellence* of IgA-producing PCs and thus their potential role in tumor progression was analyzed in the transition from normal to dysplastic epithelium to carcinoma. The observation that IgA-positive elements were densely distributed in areas of low grade dysplasia compared with normal and invasive carcinoma sites, both in the mouse and in humans, leads to hypothesize that IgA<sup>+</sup> PCs might play a role in the initial phases of colonic carcinogenesis, characterized by low grade dysplastic lesions, rather than in the overt stages of malignant transformation in which the cancer exerts its invasive potential. This result supports a concept now widely discussed in the literature that is the urgent need to understand the exact function of IgA<sup>+</sup> PCs in shaping the immune response in both the gut and extra-intestinal sites.<sup>55,56</sup>

In summary, our study shows that the tumor macroenvironment that develops following adenoma burden in the *Apc*<sup>Min/+</sup> model of CRC has a profound effect on the B cell population also in distal anatomic sites. Deepening our knowledge on this topic is essential to design specific therapies, targeted to the switching of B cells to an anti-, rather than pro-, tumoral phenotype.

## Materials and methods

### Animals and cell isolation from mouse tissues

C57BL/6J Wt and C57BL/6J-*Apc*<sup>Min/+</sup> mice were purchased from the Jackson laboratory. Breeding colonies of these animals were established and maintained under specific pathogen-free conditions at the animal facility of the Humanitas Clinical and Research Center, Milan. 10- and 18-weeks old male *Apc*<sup>Min/+</sup> mice, together with age- and gender-matched Wt littermates, were used in this study. For the induction of colitis-associated carcinoma, Wt C57BL/6J mice (8-weeks old) were given a single intraperitoneal injection of AOM (Sigma-Aldrich; 10 mg/kg body weight diluted in saline) and, after 7 days, were subjected to a 5-day exposure to drinking water containing 2.5% DSS (MP Biomedicals; MW 36.000–50.000) followed by a 14-day exposure to normal drinking water. This cycle was repeated 3 times and animals were euthanized at the conclusion of the treatment course. 9-weeks old female BALB/c mice (Harlan Laboratories) were maintained in our animal facilities and subcutaneously injected with  $2 \times 10^5$  CT-26 tumor cells. CT-26

tumor-bearing mice, and respective controls, were euthanized within 3 weeks from inoculation.

Single cell suspensions of spleen and LNs were obtained by mechanical dissociation of organs through 70  $\mu$ m-pore-size nylon filters. Red blood cells in spleen samples were lysed with ACK lysing buffer (Lonza). Peritoneal cells were obtained injecting cold PBS supplemented with 3% FBS in the peritoneal cavity and dislodging any attached cell by massaging the peritoneum. Facial vein phlebotomy was performed for blood sampling into tubes without additives and serum was obtained following a 2-step centrifugation method.

All animal experiments were performed in accordance with the animal care and use committees of the respective institutes.

### Adenoma counting and histopathological analysis

Following mouse euthanasia, the intestine was collected, fixed in formalin and embedded in paraffin. Tissue samples were cut in 4  $\mu$ m-thick sections, stained with hematoxylin/eosin (Dako) and analyzed by a blinded pathologist.

### Immunohistochemistry and immunofluorescence

Colon biopsy specimens from 10 patients were collected from the archives of the Human Pathology Section, Department of Health Science, University of Palermo, and areas of normal undamaged mucosa, low-grade dysplasia and invasive carcinoma were analyzed. Samples were fixed in 10% buffered formalin and paraffin embedded. All procedures were in accordance with the Helsinki Declaration. For *in situ* single-marker immunohistochemical analysis, 4  $\mu$ m-thick tissue sections were deparaffinized and rehydrated. Ag unmasking was performed using Novocastra Epitope Retrieval Solutions pH 6 and pH 9 (Leica Biosystems) in a PT Link pre-treatment module (Dako) at 98°C for 30 min. Sections were then brought to room temperature (RT) and washed in PBS. After neutralization of the endogenous peroxidase with 3% H<sub>2</sub>O<sub>2</sub> and Fc blocking by a specific protein block (Novocastra, Leica Biosystems), samples were incubated overnight (o/n) at 4°C with the following primary Abs: mouse monoclonal anti-human CD20 (clone L26, 1/100 dilution), mouse monoclonal anti-human CD138 (clone MI15, 1/50 dilution), rabbit polyclonal anti-human IgA (1/200 dilution), mouse monoclonal anti-human IgG (clone RWP49, 1/200 dilution), all from Leica Biosystems. Staining was revealed by polymer detection kit (Novocastra, Leica Biosystems) and 3,3'-diaminobenzidine tetrahydrochloride (DAB) substrate-chromogen. Slides were counterstained with Harris Hematoxylin (Novocastra, Leica Biosystems). Sections were analyzed under the Axio Scope A1 optical microscope (Zeiss) and microphotographs were collected through the AxioCam 503 color digital camera (Zeiss) using the Zen2 software. The quantitative analysis of stained sections was performed by counting the absolute number of positive cells out of 5 high-power microscopic fields (40x).

For the immunohistochemical analysis of IgA in the murine system, colon sections were deparaffinized, hydrated, and subjected to Ag retrieval (EDTA pH 8, 20 min, 98°C). After endogenous peroxidase block using Peroxidized 1 (Biocare Medical), samples were incubated 1 h at RT with the HRP-conjugated

goat anti-mouse IgA  $\alpha$  chain Ab (1:400, Abcam). DAB (Biocare Medical) was used as a chromogen and slides were counterstained with Mayer Emallume (Bio Optica). The quantitative analysis of stained sections was performed by counting the absolute number of positive cells out of 10 high-power microscopic fields (20x).

### Cell preparation and B/MDSC co-culture conditions

Mouse CD19 MicroBeads (Miltenyi) were used for the positive selection of B lymphocytes from total peritoneal cells. The B cell isolation kit (Miltenyi) was used to isolate B lymphocytes from total splenocytes. Purified splenic B cells were cultured at the final concentration of  $10^6$  cell/mL, in the presence or absence of 1  $\mu$ g/mL anti-mouse CD40 mAb (BD Pharmingen), 10  $\mu$ g/mL LPS (Sigma-Aldrich) or 5  $\mu$ g/mL CpG (Sigma-Aldrich). After 48 h, necrotic and apoptotic cells were detected by staining with annexin V and propidium iodide (annexin V-FITC apoptosis detection kit; eBioscience), followed by flow cytometry analysis. Cell supernatants were collected and the levels of IL-10 and LAP-1 quantified by ELISA (eBioscience). In certain experiments, B cells were labeled by incubation with 5  $\mu$ mol/L CFSE (Invitrogen-Molecular Probes) for 15 min at 37°C and cell proliferation was assessed by flow cytometry after 72 h of culture.

CD11b<sup>+</sup>Gr-1<sup>+</sup> myeloid cells were isolated using magnetic cell sorting. Splenocytes were first incubated with the anti-Gr-1-biotin Ab and, after washing, with streptavidin microbeads (both from Miltenyi). The positive fraction (all CD11b<sup>+</sup>; Fig. 6B) was separated by passage through LS MACS columns (Miltenyi) and used for the co-culture experiments with B lymphocytes. The 2 cell types were plated in a 1:1 ratio, in the presence or absence of 1  $\mu$ g/mL LPS, which acts as an activatory signal on both populations.

### Immunophenotyping

Single cell suspensions were surface stained using the anti-mouse mAbs listed in Table S2. Immunofluorescent staining of IL-10 was performed on leukocytes isolated from spleen, peritoneum and LNs and on CD40-activated B lymphocytes. Cells were resuspended in medium containing 10  $\mu$ g/mL LPS, 50 ng/mL PMA (Sigma-Aldrich), 500 ng/mL ionomycin (Sigma-Aldrich) and 2  $\mu$ mol/L monensin (eBioscience), and cultured for 5 h at 37°C. IL-10 intracellular staining was performed as described previously.<sup>25</sup> Samples stained for IL-10 also allowed the evaluation of the percentages of viable B cells among total leukocytes since a dual staining with the Live/Dead Fixable Green Dead Cell Stain Probe (Invitrogen-Molecular Probes) and an anti-CD19 mAb was part of the protocol. For Ki-67 detection, total LN cell suspension was incubated for 15 min at 4°C in the dark with the green Live/Dead probe and, sequentially, with the purified anti-mouse CD16/CD32 mAb (clone 2.4G2; BD Pharmingen). Following CD19 staining, 3 mL of cold 70% ethanol was added drop by drop to the cell pellet while vortexing. Samples were incubated at -20°C for 1 h and, after 3 washes with PBS, cells were stained with PE anti-mouse Ki-67 (clone 16A8; BioLegend) following manufacturer's instructions.

Stained samples were acquired on FACScan or FACSCalibur (BD Biosciences) and data were analyzed with FlowJo software (Tree Star).

### RNA isolation and real-time PCR

Total RNA was extracted using EuroGold Trifast reagent (EuroClone), following manufacturer's instructions. RNA (1  $\mu$ g) was reverse transcribed to cDNA using the SensiFAST cDNA synthesis kit (Bioline). The generated cDNA was amplified by quantitative real-time PCR (qPCR) with the Bio-Rad CFX96 device and using SYBR green as detection agent (iQ<sup>TM</sup> SYBR Green Super Mix, Bio-Rad). Each reaction was performed in triplicate and data were collected and analyzed by the complementary computer software (CFX Manager software, Bio-Rad). G3PDH transcript levels were used to normalize samples. Primers used for qPCR were from Sigma-Aldrich and their sequences are listed in Table S3.

### Quantification of secreted IgM, IgG and IgA isotypes

The concentration of IgM, IgG and IgA in cell supernatants or mouse sera was assessed by ELISA. For the detection of the IgM isotype, the mouse IgM Ready-SET-Go! kit (eBioscience) was used. In the case of IgG and IgA a home-made sandwich ELISA was developed. Briefly, 96-well flat-bottom polystyrene plates (Corning) were coated with affinity-purified anti-mouse IgA (SouthernBiotech) or anti-mouse IgG (Sigma-Aldrich) Abs at the final concentration of 2  $\mu$ g/mL and 10  $\mu$ g/mL, respectively. After 1 h incubation at 37°C, plates were washed with 0.05% Tween 20 in PBS and blocked with 1% bovine serum albumin in PBS for 1 h at RT. 100  $\mu$ L of cell supernatants or of opportunistically diluted mouse sera were added to Ab-coated wells. Purified mouse IgA (BD Pharmingen) or IgG (Sigma-Aldrich) were used as standards. After o/n incubation at 4°C, plates were washed and optimal concentration of horseradish peroxidase-conjugated goat anti-mouse IgA (SouthernBiotech; 1:2000) or goat anti-mouse IgG (Pierce; 1:1000) Abs were added. Next, plates were incubated for 1 h at RT and washed before the addition of tetramethylbenzidine substrate solution (Sigma-Aldrich). The reaction was stopped with 2 mol/L sulfuric acid and absorbance was measured at 450 nm.

### Statistical analyses

Results are presented as mean  $\pm$  SEM and data analysis was performed with the Prism GraphPad Software. For comparisons between 2 groups the 2-tailed unpaired and paired Student's *t*-tests were used. When multiple comparisons were necessary, data were analyzed with the one-way ANOVA test and the Bonferroni correction was used as *post-hoc* analysis. In all tests, *p* values < 0.05 were considered statistically significant.

### Disclosure of potential conflicts of interest

No potential conflicts of interest were disclosed.

## Acknowledgment

The authors thank Dr. Luca Danelli for critical reading and suggestions.

## Funding

This work was supported by Associazione Italiana Ricerca sul Cancro (AIRC) under grant IG 2014 N.15561; Progetti di Ricerca di Interesse Nazionale (PRIN) under grant 2015YYKPNN\_003 and Associazione Italiana Mastocitosi (ASIMAS) under grant 10754 to C.P.; and by My First AIRC Grant (MFAG) 2015 under grant 17795 and Fondazione Cariplo per la Ricerca under grant 2012/0678 to S.V.

## ORCID

Stefania Vetrano  <http://orcid.org/0000-0001-9825-2000>  
 Andrea Piontini  <http://orcid.org/0000-0002-9963-5502>  
 Alessia Burocchi  <http://orcid.org/0000-0001-8269-0460>  
 Barbara Frossi  <http://orcid.org/0000-0001-9855-2396>  
 Claudio Tripodo  <http://orcid.org/0000-0002-0821-6231>  
 Mario P. Colombo  <http://orcid.org/0000-0003-0042-7955>  
 Carlo E. Pucillo  <http://orcid.org/0000-0002-4872-6156>

## References

- Pancione M, Giordano G, Remo A, Febraro A, Sabatino L, Manfrin E, Ceccarelli M, Colantuoni V. Immune escape mechanisms in colorectal cancer pathogenesis and liver metastasis. *J Immunol Res* 2014; 2014 (2014):1-11; PMID:24741617; <https://doi.org/10.1155/2014/686879>
- de Vries NL, Swets M, Vahrmeijer AL, Hokland M, Kuppen PJ. The immunogenicity of colorectal cancer in relation to tumor development and treatment. *Int J Mol Sci* 2016; 17(7):E1030; PMID:27367680; <https://doi.org/10.3390/ijms17071030>
- Markman JL, Shiao SL. Impact of the immune system and immunotherapy in colorectal cancer. *J Gastrointest Oncol* 2015; 6(2):208-23; PMID:25830040; <https://doi.org/10.3978/j.issn.2078-6891.2014.077>
- Di Caro G, Marchesi F, Laghi L, Grizzi F. Immune cells: Plastic players along colorectal cancer progression. *J Cell Mol Med* 2013; 17(9):1088-95; PMID:24151976; <https://doi.org/10.1111/jcmm.12117>
- Rutkowski MR, Svoronos N, Perales-Puchalt A, Conejo-Garcia JR. The tumor microenvironment: Cancer-promoting networks beyond tumor beds. *Adv Cancer Res* 2015; 128:235-62; PMID:26216635; <https://doi.org/10.1016/bs.acr.2015.04.011>
- Kobayashi T, Hamaguchi Y, Hasegawa M, Fujimoto M, Takehara K, Matsushita T. B cells promote tumor immunity against B16F10 melanoma. *Am J Pathol* 2014; 184(11):3120-9; PMID:25173132; <https://doi.org/10.1016/j.ajpath.2014.07.003>
- Forte G, Sorrentino R, Montinaro A, Luciano A, Adcock IM, Maiolino P, Arra C, Cicala C, Pinto A, Morello S. Inhibition of CD73 improves B cell-mediated anti-tumor immunity in a mouse model of melanoma. *J Immunol* 2012; 189(5):2226-33; PMID:22826317; <https://doi.org/10.4049/jimmunol.1200744>
- Zhang Y, Gallastegui N, Rosenblatt JD. Regulatory B cells in anti-tumor immunity. *Int Immunol* 2015; 27(10):521-30; PMID:25999597; <https://doi.org/10.1093/intimm/dxv034>
- Shah S, Divekar AA, Hilchey SP, Cho HM, Newman CL, Shin SU, Nechustan H, Challita-Eid PM, Segal BM, Yi KH, et al. Increased rejection of primary tumors in mice lacking B cells: Inhibition of anti-tumor CTL and TH1 cytokine responses by B cells. *Int J Cancer* 2005; 117(4):574-86; PMID:15912532; <https://doi.org/10.1002/ijc.21177>
- Tadmor T, Zhang Y, Cho HM, Podack ER, Rosenblatt JD. The absence of B lymphocytes reduces the number and function of T-regulatory cells and enhances the anti-tumor response in a murine tumor model. *Cancer Immunol Immunother* 2011; 60(5):609-19; PMID:21253724; <https://doi.org/10.1007/s00262-011-0972-z>
- Zhang Y, Eliav Y, Shin SU, Schreiber TH, Podack ER, Tadmor T, Rosenblatt JD. B lymphocyte inhibition of anti-tumor response depends on expansion of Treg but is independent of B-cell IL-10 secretion. *Cancer Immunol Immunother* 2013; 62(1):87-99; PMID:22772949; <https://doi.org/10.1007/s00262-012-1313-6>
- Milne K, Kobel M, Kalloger SE, Barnes RO, Gao D, Gilks CB, Watson PH, Nelson BH. Systematic analysis of immune infiltrates in high-grade serous ovarian cancer reveals CD20, FoxP3 and TIA-1 as positive prognostic factors. *PLoS One* 2009; 4(7):e6412; PMID:19641607; <https://doi.org/10.1371/journal.pone.0006412>
- Bouaziz JD, Yanaba K, Tedder TF. Regulatory B cells as inhibitors of immune responses and inflammation. *Immunol Rev* 2008; 224(1):201-14; PMID:18759928; <https://doi.org/10.1111/j.1600-065X.2008.00661.x>
- Mauri C, Menon M. The expanding family of regulatory B cells. *Int Immunol* 2015; 27(10):479-86; PMID:26071023; <https://doi.org/10.1093/intimm/dxv038>
- Ray A, Wang L, Dittel BN. IL-10-independent regulatory B-cell subsets and mechanisms of action. *Int Immunol* 2015; 27(10):531-6; PMID:25999596; <https://doi.org/10.1093/intimm/dxv033>
- Shimabukuro-Vornhagen A, Schlosser HA, Gryschock L, Malcher J, Wennhold K, Garcia-Marquez M, Herbold T, Neuhaus LS, Becker HJ, Fiedler A, et al. Characterization of tumor-associated B-cell subsets in patients with colorectal cancer. *Oncotarget* 2014; 5(13):4651-64; PMID:25026291; <https://doi.org/10.18632/oncotarget.1701>
- Berntsson J, Nodin B, Eberhard J, Micke P, Jirstrom K. Prognostic impact of tumour-infiltrating B cells and plasma cells in colorectal cancer. *Int J Cancer* 2016; 139(5):1129-39; PMID:27074317; <https://doi.org/10.1002/ijc.30138>
- Jackstadt R, Sansom OJ. Mouse models of intestinal cancer. *J Pathol* 2016; 238(2):141-51; PMID:26414675; <https://doi.org/10.1002/path.4645>
- Kitahara S, Suzuki Y, Morishima M, Yoshii A, Kikuta S, Shimizu K, Morikawa S, Sato Y, Ezaki T. Vasohibin-2 modulates tumor onset in the gastrointestinal tract by normalizing tumor angiogenesis. *Mol Cancer* 2014; 13:99; PMID:24885408; <https://doi.org/10.1186/1476-4598-13-99>
- Yamada Y, Mori H. Multistep carcinogenesis of the colon in Apc (Min/+) mouse. *Cancer Sci* 2007; 98(1):6-10; PMID:17052257; <https://doi.org/10.1111/j.1349-7006.2006.00348.x>
- Swamy MV, Patlolla JM, Steele VE, Kopelovich L, Reddy BS, Rao CV. Chemoprevention of familial adenomatous polyposis by low doses of atorvastatin and celecoxib given individually and in combination to APCMin mice. *Cancer Res* 2006; 66(14):7370-7; PMID:16849589; <https://doi.org/10.1158/0008-5472.CAN-05-4619>
- Coletta PL, Muller AM, Jones EA, Muhl B, Holwell S, Clarke D, Meade JL, Cook GP, Hawcroft G, Ponchel F, et al. Lymphodepletion in the ApcMin/+ mouse model of intestinal tumorigenesis. *Blood* 2004; 103(3):1050-8; PMID:14525778; <https://doi.org/10.1182/blood-2003-03-0707>
- You S, Ohmori M, Pena MM, Nassri B, Quito J, Al-Assad ZA, Liu L, Wood PA, Berger SH, Liu Z, et al. Developmental abnormalities in multiple proliferative tissues of Apc(Min/+) mice. *Int J Exp Pathol* 2006; 87(3):227-36; PMID:16709231; <https://doi.org/10.1111/j.1365-2613.2006.00477.x>
- DiLillo DJ, Matsushita T, Tedder TF. B10 cells and regulatory B cells balance immune responses during inflammation, autoimmunity, and cancer. *Ann N Y Acad Sci* 2010; 1183(1):38-57; PMID:20146707; <https://doi.org/10.1111/j.1749-6632.2009.05137.x>
- Yanaba K, Bouaziz JD, Matsushita T, Tsubata T, Tedder TF. The development and function of regulatory B cells expressing IL-10 (B10 cells) requires antigen receptor diversity and TLR signals. *J Immunol* 2009; 182(12):7459-72; PMID:19494269; <https://doi.org/10.4049/jimmunol.0900270>
- Mauri C, Bosma A. Immune regulatory function of B cells. *Annu Rev Immunol* 2012; 30:221-41; PMID:22224776; <https://doi.org/10.1146/annurev-immunol-020711-074934>
- Ganti SN, Albershardt TC, Iritani BM, Ruddell A. Regulatory B cells preferentially accumulate in tumor-draining lymph nodes and promote tumor growth. *Sci Rep* 2015; 5:12255; PMID:26193241; <https://doi.org/10.1038/srep12255>
- Mion F, Tonon S, Toffoletto B, Cesselli D, Pucillo CE, Vitale G. IL-10 production by B cells is differentially regulated by immune-mediated



- and infectious stimuli and requires p38 activation. *Mol Immunol* 2014; 62(2):266-76; PMID:24970737; <https://doi.org/10.1016/j.molimm.2014.05.018>
29. Lampropoulou V, Hoehlig K, Roch T, Neves P, Calderon Gomez E, Sweenie CH, Hao Y, Freitas AA, Steinhoff U, Anderton SM, et al. TLR-activated B cells suppress T cell-mediated autoimmunity. *J Immunol* 2008; 180(7):4763-73; PMID:18354200; <https://doi.org/10.4049/jimmunol.180.7.4763>
  30. Amano M, Baumgarth N, Dick MD, Brossay L, Kronenberg M, Herzenberg LA, Strober S. CD1 expression defines subsets of follicular and marginal zone B cells in the spleen: Beta 2-microglobulin-dependent and independent forms. *J Immunol* 1998; 161(4):1710-7; PMID:9712035.
  31. Mauri C, Blair PA. Regulatory B cells in autoimmunity: Developments and controversies. *Nat Rev Rheumatol* 2010; 6(11):636-43; PMID:20856268; <https://doi.org/10.1038/nrrheum.2010.140>
  32. de Andres B, Cortegano I, Serrano N, del Rio B, Martin P, Gonzalo P, Marcos MA, Gaspar ML. A population of CD19highCD45R-/low-CD21low B lymphocytes poised for spontaneous secretion of IgG and IgA antibodies. *J Immunol* 2007; 179(8):5326-34; PMID:17911619; <https://doi.org/10.4049/jimmunol.179.8.5326>
  33. de Andres B, Prado C, Palacios B, Alia M, Jagtap S, Serrano N, Cortegano I, Marcos MA, Gaspar ML. Dynamics of the splenic innate-like CD19(+)/CD45Rlo cell population from adult mice in homeostatic and activated conditions. *J Immunol* 2012; 189(5):2300-8; PMID:22837485; <https://doi.org/10.4049/jimmunol.1200224>
  34. Underhill GH, Kolli KP, Kansas GS. Complexity within the plasma cell compartment of mice deficient in both E- and P-selectin: Implications for plasma cell differentiation. *Blood* 2003; 102(12):4076-83; PMID:12881311; <https://doi.org/10.1182/blood-2003-03-0947>
  35. Culton DA, O'Conner BP, Conway KL, Diz R, Rutan J, Vilen BJ, Clarke SH. Early preplasma cells define a tolerance checkpoint for autoreactive B cells. *J Immunol* 2006; 176(2):790-802; PMID:16393962; <https://doi.org/10.4049/jimmunol.176.2.790>
  36. Lazarus NH, Kunkel EJ, Johnston B, Wilson E, Youngman KR, Butcher EC. A common mucosal chemokine (mucosae-associated epithelial chemokine/CCL28) selectively attracts IgA plasmablasts. *J Immunol* 2003; 170(7):3799-805; PMID:12646646; <https://doi.org/10.4049/jimmunol.170.7.3799>
  37. Bronte V, Brandau S, Chen SH, Colombo MP, Frey AB, Greten TF, Mandruzzato S, Murray PJ, Ochoa A, Ostrand-Rosenberg S, et al. Recommendations for myeloid-derived suppressor cell nomenclature and characterization standards. *Nat Commun* 2016; 7:12150; PMID:27381735; <https://doi.org/10.1038/ncomms12150>
  38. Gabrilovich DI, Bronte V, Chen SH, Colombo MP, Ochoa A, Ostrand-Rosenberg S, Schreiber H. The terminology issue for myeloid-derived suppressor cells. *Cancer Res* 2007; 67(1):425; PMID:17210725; <https://doi.org/10.1158/0008-5472.CAN-06-3037>
  39. Jordan MB, Mills DM, Kappler J, Marrack P, Cambier JC. Promotion of B cell immune responses via an alum-induced myeloid cell population. *Science* 2004; 304(5678):1808-10; PMID:15205534; <https://doi.org/10.1126/science.1089926>
  40. Crook KR, Jin M, Weeks MF, Rampersad RR, Baldi RM, Glekas AS, Shen Y, Esserman DA, Little P, Schwartz TA, et al. Myeloid-derived suppressor cells regulate T cell and B cell responses during autoimmune disease. *J Leukoc Biol* 2015; 97(3):573-82; PMID:25583578; <https://doi.org/10.1189/jlb.4A0314-139R>
  41. Xu X, Meng Q, Erben U, Wang P, Glauben R, Kuhl AA, Wu H, Ma CW, Hu M, Wang Y, et al. Myeloid-derived suppressor cells promote B-cell production of IgA in a TNFR2-dependent manner. *Cell Mol Immunol* 2016; 13:1-10; PMID:26658640; <https://doi.org/10.1038/cmi.2015.103>
  42. Leslie A, Carey FA, Pratt NR, Steele RJ. The colorectal adenoma-carcinoma sequence. *Br J Surg* 2002; 89(7):845-60; PMID:12081733; <https://doi.org/10.1046/j.1365-2168.2002.02120.x>
  43. Muthuswamy RV, Sundstrom P, Borjesson L, Gustavsson B, Quiding-Jarbrink M. Impaired migration of IgA-secreting cells to colon adenocarcinomas. *Cancer Immunol Immunother* 2013; 62(6):989-97; PMID:23591979; <https://doi.org/10.1007/s00262-013-1410-1>
  44. Rognum TO, Brandtzaeg P, Orjasaeter H, Eljjo K, Hognestad J. Immunohistochemical study of secretory component, secretory IgA and carcinoembryonic antigen in large bowel carcinomas. *Pathol Res Pract* 1980; 170(1-3):126-45; PMID:18788158; [https://doi.org/10.1016/S0344-0338\(80\)80161-0](https://doi.org/10.1016/S0344-0338(80)80161-0)
  45. Al-Zoughbi W, Huang J, Paramasivan GS, Till H, Pichler M, Guertl-Lackner B, Hoefler G. Tumor macroenvironment and metabolism. *Semin Oncol* 2014; 41(2):281-95; PMID:24787299; <https://doi.org/10.1053/j.seminoncol.2014.02.005>
  46. Castano Z, Tracy K, McAllister SS. The tumor macroenvironment and systemic regulation of breast cancer progression. *Int J Dev Biol* 2011; 55(7-9):889-97; PMID:22161844; <https://doi.org/10.1387/ijdb.1133666z>
  47. Tang A, Dadaglio G, Oberkampf M, Di Carlo S, Peduto L, Laubreton D, Desrues B, Sun CM, Montagutelli X, Leclerc C. B cells promote tumor progression in a mouse model of HPV-mediated cervical cancer. *Int J Cancer* 2016; 139(6):1358-71; PMID:27130719; <https://doi.org/10.1002/ijc.30169>
  48. Zigmund E, Halpern Z, Elinav E, Brazowski E, Jung S, Varol C. Utilization of murine colonoscopy for orthotopic implantation of colorectal cancer. *PLoS One* 2011; 6(12):e28858; PMID:22174916; <https://doi.org/10.1371/journal.pone.0028858>
  49. Balkwill FR, Capasso M, Hagemann T. The tumor microenvironment at a glance. *J Cell Sci* 2012; 125:5591-6; PMID:23420197; <https://doi.org/10.1242/jcs.116392>
  50. Baseler MW, Maxim PE, Veltri RW. Circulating IgA immune complexes in head and neck cancer, nasopharyngeal carcinoma, lung cancer, and colon cancer. *Cancer* 1987; 59(10):1727-31; PMID:3828945; [https://doi.org/10.1002/1097-0142\(19870515\)59:10%3c1727::AID-CNCR2820591009%3e3.0.CO;2-N](https://doi.org/10.1002/1097-0142(19870515)59:10%3c1727::AID-CNCR2820591009%3e3.0.CO;2-N)
  51. Ahmad S, Faruqi NA, Arif SH, Akhtar S. Serum immunoglobulin levels in neoplastic disorder of breast. *J Indian Med Assoc* 2002; 100(8):495-6; PMID:12675180
  52. Zan H, Cerutti A, Dramitinos P, Schaffer A, Casali P. CD40 engagement triggers switching to IgA1 and IgA2 in human B cells through induction of endogenous TGF-beta: Evidence for TGF-beta but not IL-10-dependent direct S mu->S alpha and sequential S mu->S gamma, S gamma->S alpha DNA recombination. *J Immunol* 1998; 161(10):5217-25; PMID:9820493
  53. Cerutti A. The regulation of IgA class switching. *Nat Rev Immunol* 2008; 8(6):421-34; PMID:18483500; <https://doi.org/10.1038/nri2322>
  54. Talmadge JE, Gabrilovich DI. History of myeloid-derived suppressor cells. *Nat Rev Cancer* 2013; 13(10):739-52; PMID:24060865; <https://doi.org/10.1038/nrc3581>
  55. Gommerman JL, Rojas OL, Fritz JH. Re-thinking the functions of IgA (+) plasma cells. *Gut Microbes* 2014; 5(5):652-62; PMID:25483334; <https://doi.org/10.4161/19490976.2014.969977>
  56. Leong KW, Ding JL. The unexplored roles of human serum IgA. *DNA Cell Biol* 2014; 33(12):823-9; PMID:25188736; <https://doi.org/10.1089/dna.2014.2639>